Gelatinous matrix, an original convergent evolution to cope with oligotrophy in Nassellaria (Radiolaria)

Natalia Llopis Monferrer[1,2,*], Sarah Romac[1], Manon Laget[3,4], Yasuhide Nakamura[5], Tristan Biard[4,#], Miguel M. Sandin[6,*,#]

[1]Sorbonne University, CNRS, UMR7144 Adaptation and Diversity in Marine Environment (AD2M) Laboratory, Ecology of Marine Plankton team, Station Biologique de Roscoff, Roscoff, France
[2]Monterey Bay Aquarium Research Institute, Moss Landing, CA, United States
[3] Oceanography Department, Dalhousie University, Halifax, NS, Canada
[4]LOG, Laboratoire d'Océanologie et de Géosciences, Université du Littoral Côte d'Opale, Université de Lille, CNRS, IRD, UMR8187, Wimereux, France
[5]Estuary Research Center, Shimane University, 1060, Nishikawatsu-cho, Matsue-city, Shimane-ken, 690-8504 Japan
[6]Institut de Biologia Evolutiva (CSIC-Universitat Pompeu Fabra), Passeig Marítim de la Barceloneta 37-49, 08003 Barcelona, Spain
[*]Corresponding authors
[#]Senior authors

Abstract

Radiolaria are heterotrophic protists abundant in the world's oceans playing important roles in oceanic biogeochemical cycles. Some species can host photosynthetic algae thus contributing to primary production. Such mixotrophic behaviour is believed to explain their ecological success in oligotrophic waters, notably Collodaria, a group of exclusively mixotrophic radiolarians embedded in a gelatinous matrix. Sampling oligotrophic California Current communities revealed an abundant, rarely observed population of Nassellaria of the genus *Phlebarachnium*, characterized to live within a gelatinous matrix along with Collodaria and Orodaria. Phylogenetic reconstruction of the ribosomal DNA suggests that these distantly related lineages within Nassellaria independently developed the ability to produce a gelatinous matrix ~120 million years ago. Molecular analyses identify photosynthetic symbionts as *Scrippsiella* sp., a common dinoflagellate symbiont of other planktonic groups. By matching our physical samples with their genetic signature, we identified these rarely observed organisms in global metabarcoding datasets, revealing a strong biogeographic affinity to oligotrophic water masses. Our results suggest that the gelatinous matrix is an exclusive adaptation to oligotrophic waters although further research is required to evaluate the similarities between the gelatinous matrices of Collodaria, Orodaria and *Phlebarachnium*. We hypothesize that such an original convergent evolution could increase the effective volume to weight ratio favoring prey contact and capture and provide an advantageous microenvironment for symbionts, enhancing ecological success in nutrient-depleted waters. This study advances our understanding of the evolution of eukaryotic diversity and highlights the specific advantages of certain adaptations, specifically when evolution occurs independently among various lineages.

Introduction

Among marine planktonic eukaryotic organisms, Radiolaria are diverse and highly abundant protists, widely distributed in the ocean, from tropical to polar waters [1, 2]. These protists exhibit a great range of lifestyles (solitary, colonial or with symbionts), trophic diversity (heterotrophic or mixotrophic) and tremendous morphological variability, spanning a wide range of sizes, from micrometers to several millimeters [3, 4]. Among the phylogenetic groups of Radiolaria, Acantharia [5] is the sole group of Radiolaria bearing a strontium sulfate skeleton, while the Polycystines group possesses an opaline silica skeleton [6]. In the Polycystines group, Spumellaria [7] exhibits concentric and spherical shapes, while Nassellaria [8] showcases a diverse range of features. These include conical skeletons and a limited number of spicules, or even large colonies of naked or silicified skeletons, akin to that found in the Collodaria group [9], or large individual skeletons as found in the Orodaria group [10]. Such an extensive diversity makes Radiolaria an ideal lineage for investigating adaptive evolution in protists.

The success of Radiolaria to adapt to diverse environments has made them important contributors of contemporary biogeochemical cycles. They can participate in the transformation of sinking particles and have been identified as a critical source of organic carbon [11, 12]. Global models indicate that Rhizaria, including Collodaria among other protists, may constitute up to 20% of the biomass of the euphotic layer (0-200m) [13], although recent estimates suggest their global biomass in the epipelagic oceans is relatively low [14]. Despite this, they can play a substantial role in zooplankton abundance, contributing up to 33% [1]. In some areas, Radiolaria may dominate the eukaryotic community recovered from metabarcoding analyses of sediment traps based below the euphotic layer [15, 16]. Besides, they also have an essential role in the silicon cycle, as many representatives take up silicic acid from the seawater to form their skeleton [17] contributing ~ 20% to the biogenic silica production of the global ocean [18]. It is because of their intricate mineral skeleton made of opaline silica that Radiolaria have left behind a continuous fossil record since the Cambrian, more than 500 Million years ago (Mya) [19], and have been instrumental for paleoenvironmental reconstructions [20, 21].

Among the most conspicuous adaptations in Radiolaria are the various types of trophic modes and feeding strategies. Some Radiolaria feed upon sinking particles while others are active predators. They use a network of cytoplasmic extensions (i.e., pseudopods) to capture and entangle a wide range of prey, from bacteria to multicellular heterotrophs like nauplii larvae [3, 22], even in oligotrophic waters where prey abundance is scarce. Many are mixotrophs harboring

photosynthetic algae [23–25]. These symbionts can be found either directly inside the organism, as in Acantharia [26], or scattered on a gelatinous organic matrix surrounding the skeleton as in Collodaria [27]. The presence of photosymbionts in these organisms contributes to primary production. In the upper 20 m of the central North Pacific, Acantharia alone can contribute up to 4% of total primary production and up to 20% of surface production [28, 29]. It has been suggested that such symbiotic adaptations were triggered by long periods of accentuated oceanic oligotrophy in the Jurassic (ca. 175-93 Mya; [5]).

In contemporary oceans, mixotrophy allows Radiolaria to thrive in various environments. Collodaria are an important component of zooplankton biomass in the epipelagic [1] and are most abundant in tropical latitudes and nutrient-impoverished waters [30]. Conversely, other Radiolaria, such as Acantharia or Spumellaria, are better adapted to meso- and eutrophic waters, richer in nutrients. These differences in biogeographical patterns have been attributed to the coloniality of Collodaria in which all individual cells share nutrients among the colony through the gelatinous matrix [27]. The presence of the gelatinous matrix could be a crucial advantage in enabling them to survive and thrive abundantly in oligotrophic waters, where prey are scarce. The gelatinous matrix also provides a conducive environment for hosting symbionts while facilitating resource optimization and adaptation strategies that contribute to the survival and ecological success of the cell. Indeed, other marine organisms, such as *Phaeocystis* algae, can also form an extracellular matrix that can host bacteria [31, 32], providing a nutrient-rich and protective environment and allowing them to form blooms and dominate the planktonic community.

In an oligotrophic environment, we collected several Nassellaria specimens embedded in a gelatinous matrix. To our knowledge, only one other study has documented these specimens, originally described as *Sethoconus myxobrachia* [33], yet recently reassigned to the genus *Phlebarachnium* [34]. We present here findings on the phylogenetic relationships and global biogeography of *Phlebarachnium*. Our approach involved sequencing rDNA genes, characterisation of the surrounding waters where these specimens were collected, and the analyses of metabarcoding datasets (Eubank; [35]). Here we hypothesize that the gelatinous matrix serves as an ecological adaptation to oligotrophy, as we observed it evolved independently in the Collodaria lineage and in the Nassellaria genus. This gelatinous matrix would increase cell volume, facilitating the capture and storage of scarce prey and nutrients. Additionally, it offers larger cellular space to host an increased number of symbionts providing an optimal environment for them, here identified within the genus *Scrippsiella*.

108

Material and Methods

Sample collection

Samples were collected during the P2107 California Current Ecosystem Long Term Ecological Research (CCE-LTER) cruise in the summer of 2021 aboard the R/V *Roger Revelle* (Fig. 1A). The sampling strategy was designed around 3 multi-day quasi-lagrangian cycles. Each cycle involved following the drift trajectories of experimental arrays, aiming to sample the same water mass. Individual casts of Conductivity, Temperature and Depth (CTD) were conducted at each station (~about 10 per cycle). Discrete bottle samples were collected at various depths from each station to measure nutrients (silicic acid ($Si(OH)_4$) and nitrate (NO_3^-)). Water column nutrient samples were measured following the standard operating procedures from the CCE-LTER. Briefly, macronutrient samples were collected and filtered through a 0.2-µm capsule filter before being frozen at -20°C for on-shore autoanalyzer analysis.

In this study, we present results from a subset of 4 stations of Cycle 3 (3-6 August), sampled in oligotrophic waters, where Nassellaria identified as *Phlebarachnium* according to [27] were identified (**Sup Fig. S1**). Plankton samples were collected using a ringnet (200-µm mesh size, mouth diameter: 1 m) towed vertically from 50 m to the surface and from 300 m to the surface at each sampling location. *Phlebarachnium* specimens were also collected from vertically stratified sampling collected with a 1 m^2, 202-µm mesh MOCNESS.

Immediately after collection, each net sample was observed using a stereomicroscope (Zeiss Stemi 508) and images of targeted organisms were captured using a Canon Eos 77D camera. Morphological measurements, including major and minor axes of individual cells, and their skeleton area, were obtained using ImageJ software [36, 37] to estimate the biovolume of the cells (**Sup Table S1**). Each specimen was transferred into 1.5 ml Eppendorf tubes containing 50 µl of molecular grade absolute ethanol and stored at -20˚C until DNA extraction. Scanning electron microscopy images were captured using a S-3400N Hitachi scanning electron microscope following the protocol in [38] for detailed examination of morphology.

DNA extraction and sequencing

DNA was extracted using the MasterPure Complete DNA and RNA Purification Kit (Epicentre) following the manufacturer's instructions. Partial 28S rDNA (D1 and D2 regions) was amplified by

138 Polymerase Chain Reaction (PCR) using Radiolaria and Nassellaria specific primers (28S-Nas-
139 F: 5' - AGT AAC GGC GAG TGA AGC - 3' and 28S-Nas-R: 5' - CCA ACA TAC DTG CTC TTG T
140 - 3'). For further details about rDNA amplification see [8]. PCR amplicons were visualized on 1%
141 agarose gel stained with ethidium bromide. Positive reactions were purified using the Nucleospin
142 Gel and PCR Clean up kit (Macherey Nagel), following manufacturer's instructions and sent to
143 Macrogen Europe for sequencing. After sequencing, forward and reverse sequences were
144 checked and assembled using ChromasPro software version 2.1.4 (2017). Sequences were
145 compared to the GenBank reference database using the BLAST search tool integrated in
146 ChromasPro to discriminate radiolarian sequences from possible contamination. The presence of
147 chimeras was checked by mothur v1.39.3 [39] against the PR2 database v5.0. [40]. No chimeras
148 were found, and therefore sequences were kept for further analyses. Final sequences were
149 deposited in NCBI under the accession numbers OR978667-OR978672. Single-cell amplification
150 and sequencing of the 18S rDNA was also attempted following [8], yet after checking correct *in*
151 *silico* specificity of the primers, no successful reactions yielded 18S sequences of the Nassellaria
152 host.

153 Phylogenetic analysis

154 Our partial 28S rDNA sequences were compared against an environmental dataset [41]
155 containing near full-length sequences of the rDNA (from doi: 10.6084/m9.figshare.15164772.v3)
156 using vsearch v2.21.1 [42]. In total 2 sequences of the near full-length rDNA were identified with
157 a similarity identity of 99.8%, with the third best identity score at 89.1%. Additionally, 135
158 Nassellaria sequences were extracted from [43], with 24 Spumellaria sequences as the outgroup
159 (**Sup Table S2**). Datasets of the 18S and 28S rDNA were independently aligned with mafft [44]
160 using the L-INS-i algorithm ('—localpair') and 1000 iterative refinement cycles. The alignment was
161 visualized in AliView v1.28 [45] to check for possible artifacts and trimmed with a 5% gap threshold
162 using trimAl [46]. Final alignments contained 151 sequences with 1849 aligned positions for the
163 18S rDNA and 93 sequences with 800 positions for the partial 28S rDNA. Final datasets of the
164 18S and the partial 28S rDNA were concatenated with an in-house script freely available on
165 GitHub (MiguelMSandin/random/fasta/fastaConcat.py), resulting in 165 sequences, 2647 aligned
166 positions. Phylogenetic analyses were performed using Maximum Likelihood (ML) implemented
167 in RAxML-ng [47] and IQ-Tree [48] and a Bayesian Inference (BI) implemented in MrBayes [49].
168 RAxML-ng was run under a GTR + Gamma model of evolution over 100 parsimonious starting
169 trees and 1000 Felsenstein bootstraps. Prior to phylogenetic inference with IQ-Tree, ModelFinder

170 identified GTR + F + R4 as the best fitting model of evolution and it was therefore used over 1000
171 bootstraps and 10 independent runs. Lastly, MrBayes was run under a GTR + Gamma model of
172 evolution over 10 million generations and 4 independent runs. After checking for convergence of
173 the bayesian MCMC chain in tracer v1.7.2 a 25% burnin was applied and a strict consensus tree
174 was built.

175 While attempting 18S rDNA amplification, up to 6 different and high-quality sequences
176 taxonomically assigned to dinoflagellates were sequenced from 6 independent hosts (deposited
177 in NCBI under the accession numbers OR961112-OR961117). These sequences were combined
178 with those used in [23] in order to study the phylogenetic relationships of the potential symbionts.
179 In total 71 sequences of the 18S rDNA were aligned and trimmed (following methods stated
180 above) resulting in 1803 positions. Phylogenetic analyses were inferred in RAxML-ng and IQ-
181 Tree as mentioned above.

182 Calibration of the molecular clock

183 Divergence times among sequences were estimated in BEAST v2.7.3 [50] under the Optimized
184 Relaxed Clock [51] model to avoid assumption of substitution rates correlation between sister
185 clades, a GTR+Gamma (4 categories) model of nucleotide substitution and a Birth-Death model
186 of speciation [52]. Fossil calibrations were taken from [43], including a maximum root age of 1200
187 Ma and minimum of 500 Ma under a uniform distribution. The MCMC chain was run over 10
188 million generations sampled every 1000 states on 3 independent runs (remaining operators were
189 left as default). After completion, effective sampling size was checked to be equal or higher than
190 200 and the 3 independent runs were combined in LogCombiner v2.7.4 with a 25% burnin. The
191 final tree was summarized in TreeAnnotator v2.7.3.

192 Metabarcoding analyses

193 Global biogeographic patterns of *Phlebarachnium* were examined in the EukBank metabarcoding
194 dataset of the V4 hypervariable region of the 18S rDNA [35]. *Phlebarachnium* metabarcodes were
195 extracted from the near-full length rDNA sequences mentioned above with vsearch v2.21.1 [42].
196 In total, 2 metabarcodes from the V4 rDNA were selected and extracted from the EukBank dataset
197 with a similarity identity of 99.5% and 96.9% (the third closest metabarcode hit to our
198 *Phlebarachnium* sequences with an identity of 89.4%). Given that the abundance of the second
199 metabarcode was significantly lower than that of the first metabarcode (14 total reads compared

200 to 306522), read abundances of both metabarcodes were clustered together for biogeographic
201 patterns exploration. Only samples with a marine identifier under 'biome' were considered in this
202 study.

203 Results

204 Environmental context

205 Specimens of *Phlebarachnium* were found in highly oligotrophic waters, where Chlorophyll *a*
206 concentration was low (ranging from 0 to 9 mg m^{-3}) (Fig. 1A). At Cycle 3, fluorescence values
207 were almost negligible, except for a peak detected at around 100 m (Fig. 1B). In Cycles 1 and 2,
208 near the coast, fluorescence and Chlorophyll *a* values were much higher in the upper 100 m of
209 the water column than in Cycle 3. Nutrient concentrations (silicic acid and nitrate) in Cycles 1 and
210 2 showed an upward trend with depth from the surface waters. During Cycle 3, nutrients depletion
211 was observed in the upper 150 m of the water column. Beyond this depth, values reached 30 and
212 25 µM for silicic acid and nitrate, respectively.

213

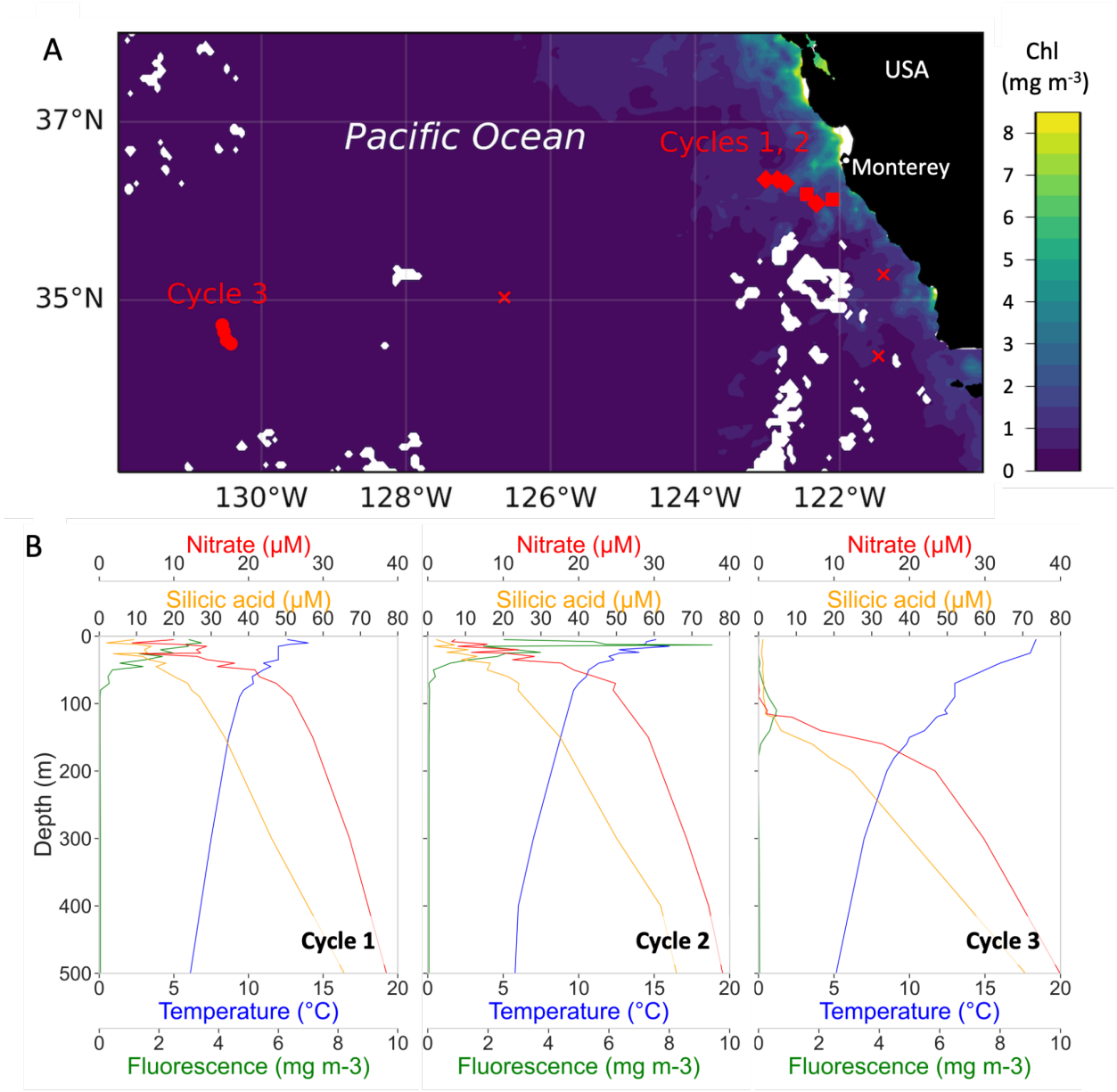

Fig. 1 (A) Map of the sampling locations of the P2107 cruise where net tows were carried out. Squares are used for Cycle 1, diamonds for Cycle 2, circles for Cycle 3 and crosses for sampling outside the cycles. Cycle 3 stations are where Nassellaria specimens used in this study were found. The color scale shows real time Aqua MODIS chlorophyll concentration (mg m^{-3}), 4 km resolution for August 2021. **(B)** Fluorescence (mg m^{-3}) and temperature (°C) data from the CTD cast and nutrients concentration (silicic acid and nitrate, in µM) for each cycle.

Morphological assessment

Based on live observations and light microscope images, two populations of *Phlebarachnium* cells were defined showing differences in average size, color and depth distribution, which we refer to as the yellow and orange populations (Fig. 2A and B, respectively). Both populations were surrounded by a gelatinous matrix. Morphometric assessments of matrix and skeleton, including major and minor axes measurements, volume and estimated spherical diameter (ESD) calculations, were conducted on 25 individuals from each population (**Sup Table S1**). The ESD of the gelatinous matrix was 845 (± 73) µm and 1383 (± 129) µm, and the skeleton ESD was 332 (± 35) µm and 563 (± 49) µm for the yellow and orange populations, respectively. A Wilcoxon test indicated that both matrix and skeleton in orange specimens were significantly larger than yellow specimens (Z=-4.37, pvalue<0.001; Z=-4.37, pvalue<0.001). The skeleton volume/matrix ratio volume varied from 3 to 12%, with no significant differences among populations (Z=-1.70, pvalue=0.09).

In approximately 15% of the specimens from the yellow population, we observed the presence of enclosed prey within the gelatinous matrix. These include mainly Harpacticoid copepods and nauplius larvae. All copepods were consistently placed near the base of the cephalis (Fig. 2C, dashed white arrow), and on many occasions we observed a clear opening within the gelatinous matrix (Fig. 2C, solid white arrow). Although we cannot conclude on the vertical distribution of these organisms due to sampling limitations, we observed some distribution patterns in depth. While host specimens of the yellow population were found in all the nets tows, from 0-50 m, from 75-150 m and 0-300 m, specimens of the orange population were only found in the deeper net tows, below 75 m.

Both populations show numerous golden-yellow bodies distributed across the gelatinous matrix, with a lower concentration in the deeper-dwelling orange population. Both populations show different distributions of these golden yellow bodies. In the yellow population, they appear strategically arranged in discrete clusters within specific and recurring regions of the matrix, which may show rounded inflations. We noted the presence of 3 to 4 clusters, with one positioned toward the apical horn and 2 to 3 arranged toward the bottom of the gelatinous matrix (Fig. 2A). In contrast, in the orange population, the symbionts are evenly distributed throughout the matrix (Fig. 2B). Despite these differences in symbiont distribution, both populations shared common features in their skeletal morphology. Each representative exhibited a reticulate shell, characterized by a spherical cephalic region and a larger bell-shaped thorax (Fig. 2D-G).

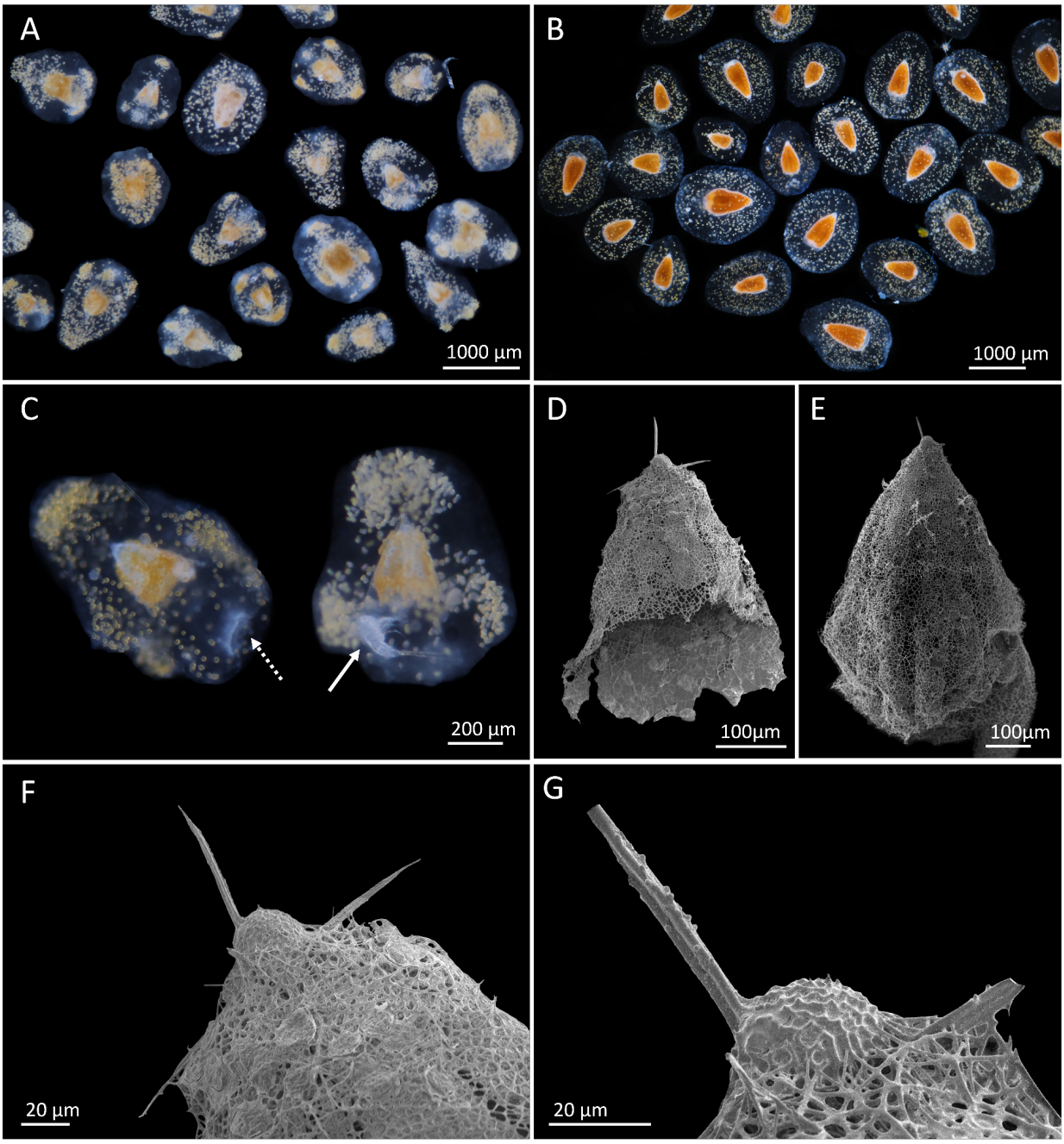

Fig. 2 (A-C) Light microscope images of living *Phlebarachnium* specimens; C is a composition of two separate images, with the dotted arrow indicating the aperture within the gelatinous matrix, and the solid arrow pointing to the prey embedded in the matrix, **(D-E)** scanning electron micrograph of the skeleton of *Phlebarachnium* specimens, with a detailed focus of the head **(F-G)** used for traditional morphological classification. A, C and E are the "yellow" population of *Phlebarachnium*. collected with the 0-50m net tow; B, C and F are the "orange" population found below 75 m.

262 # Molecular and phylogenetic analyses

263 Phylogenetic analyses revealed that *Phlebarachnium* constitute a highly supported novel clade
264 (Bootstrap Support, BS≥94; Posterior Probability, PP≥0.91) within Nassellaria and confidently
265 supported (BS=72 and 78, PP=0.98) as sister to Lithochytridoidea, Pterocorythoidea and an
266 environmental clade (a clade with no morphologically described sequences) named as Nass-4
267 (Fig. 3). This distinct *Phlebarachnium* clade shows a distant phylogenetic relatedness to Orodaria
268 and Collodaria, the only other Radiolaria group known to develop a gelatinous matrix around the
269 cells. Molecular dating estimates the last common ancestor between *Phlebarachnium* and
270 Collodaria in 362 Mya (with a Highest Posterior Density -HPD- between 436 and 299 Mya; **Sup**
271 **Fig. S2**). Orodaria and Collodaria diversified 165 Mya (HPD: 233-103). While Collodaria has been
272 dated to first diversified at 127 Mya (HPD: 166-77), *Phlebarachnium* clade first diversified 4.9 Mya
273 (HPD: 13.4-0.99), yet separated from its sister clades much earlier at 117 Mya (HPD: 179-75),
274 and Orodaria only diversifies at 1.2 Mya (HPD: 6-0.010).
275 While morphological observations identified two distinct populations, molecular analyses showed
276 no clear differentiation as all sequences obtained in our study were identical. In addition, both
277 populations show similar golden yellow bodies phylogenetically assigned to *Scrippsiella* (**Sup Fig.**
278 **S3**), a common symbiotic dinoflagellate, yet independent from the common symbiont of
279 Polycystines, *Brandtodinium*.

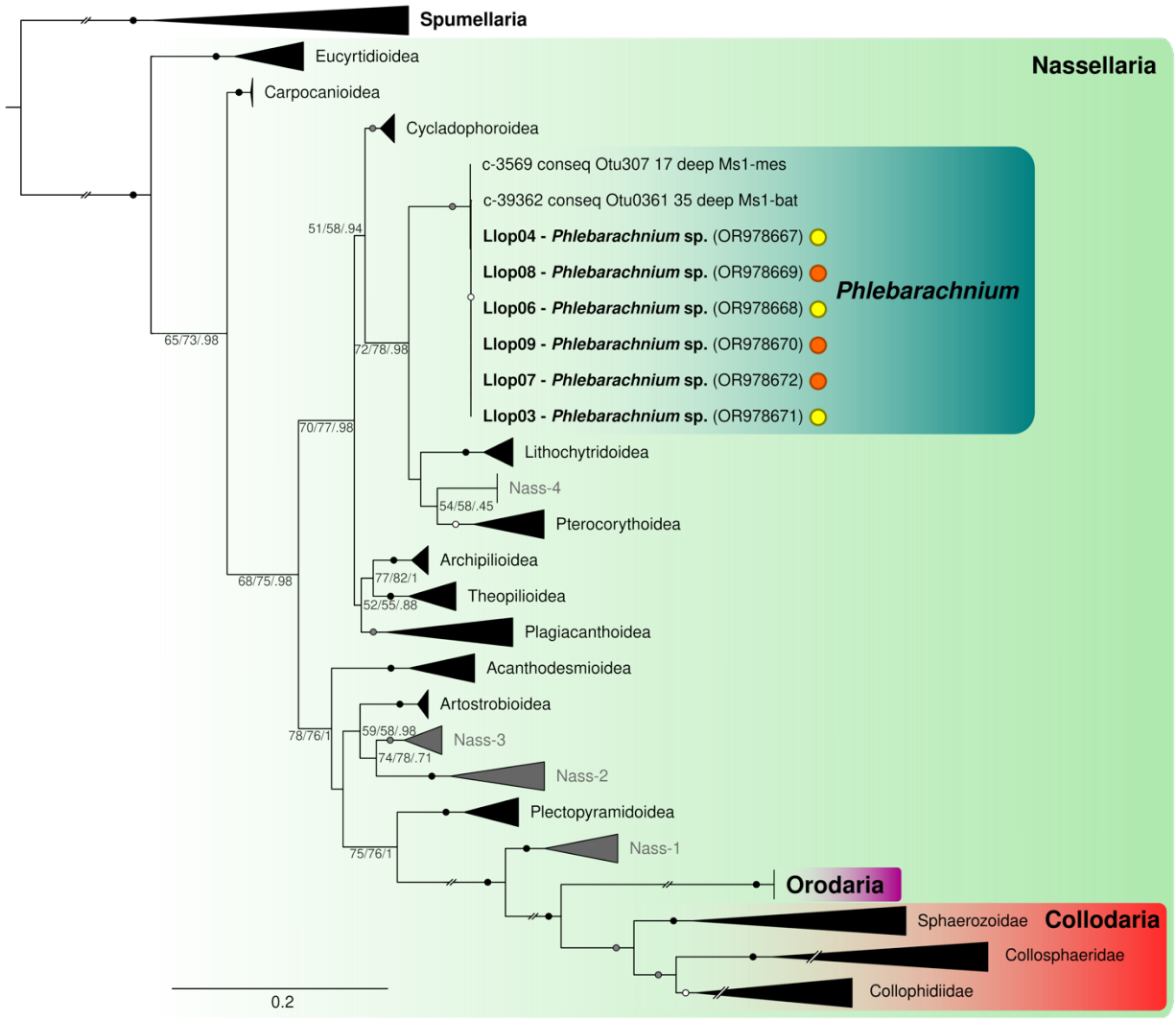

Fig. 3. Molecular phylogeny of Nassellaria inferred from the concatenated 18S and the partial 28S (D1+D2) rDNA (141 taxa and 2649 aligned positions). In total, 24 Spumellaria sequences were assembled as an outgroup. Values at nodes represent RAxML-ng (GTR+Gamma; tree shown in figure), IQ-Tree (GTR+F+F4; 10 runs) bootstrap values (BS; 1000 bootstrap each) and MrBayes (GTR+G) posterior probabilities (PP; computed after 10 million generations over 4 independent runs and 25% burnin). Only values above 50 BS and/or 0.5 PP are shown. Hollow circles at nodes indicate BS ≥ 80 and PP ≥ 0.8, filled grey circles BS ≥ 90 and PP ≥ 0.9 and filled black circles BS ≥ 99 and PP ≥ 0.99. Branches and clades with a double barred symbol have been 50% reduced for clarity. Orange and yellow circles after the *Phlebarachnium* sequence names represent whether they belong to the so-called “orange” or “yellow” populations.

Biogeographic analyses

Overall, the collection and identification of this enigmatic Radiolaria in the California Current allowed for the identification of a previously unassigned sequence in a global metabarcoding dataset. Here, we have used different sequences coming from various sources to explore global biogeographic patterns of *Phlebarachnium*, and due to their high degree of similarity (>96.9%) and the pairwise distance dissimilarity to other non-*Phlebarachnium* sequences (<89.4) we were confidentially able to taxonomically assign these reads to *Phlebarachnium* (**Fig. 4D**). Global metabarcoding analysis of the V4 hypervariable region of the rDNA shows that *Phlebarachnium* contributed on average 0.45 (±1.4) % to the total eukaryotic community across the EukBank dataset (with a median contribution of 0.02%). Yet in some samples of the Pacific Ocean, *Phlebarachnium* contributes to up to 13.41% of the total eukaryotic reads (**Fig. 4A**). The highest relative abundance of *Phlebarachnium* coincided with the oligotrophic gyres of the Pacific Ocean at ~30° of latitude (**Fig. 4B**) and in between -80° and -180° of longitude of the upper mesopelagic water mass (200-1000; **Fig. 4C**).

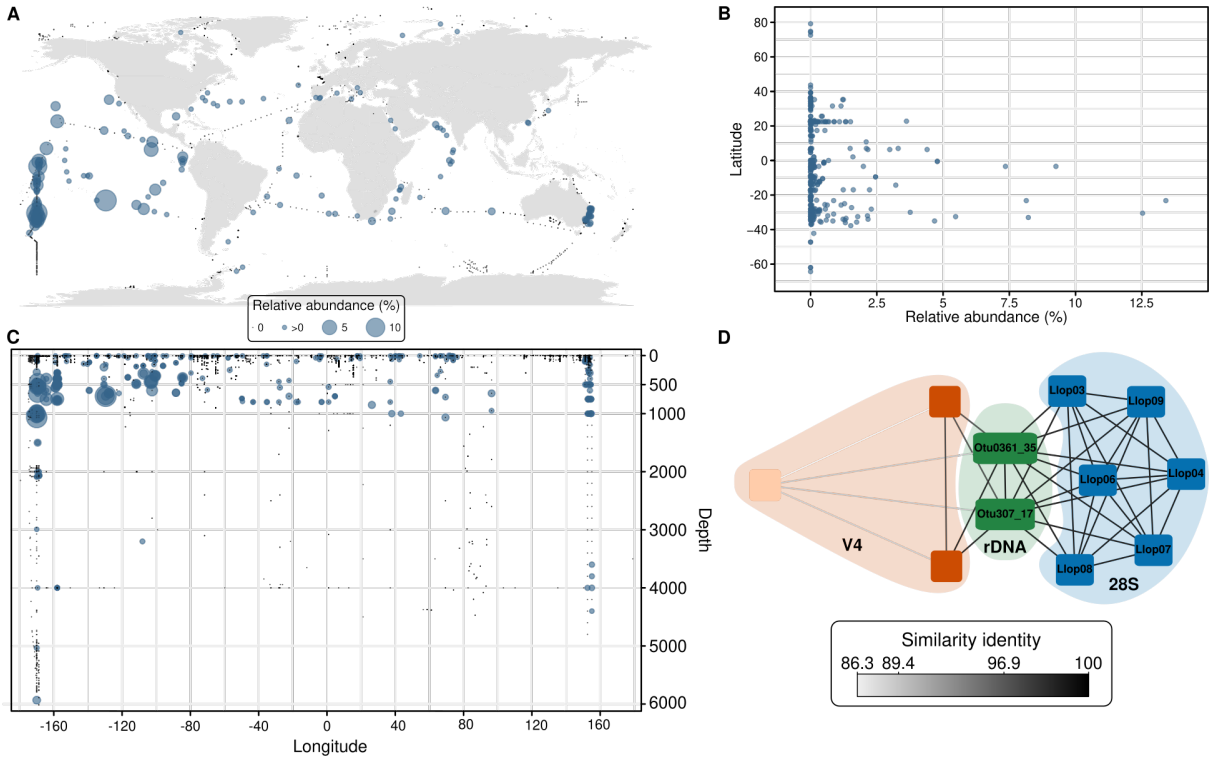

Fig. 4 Global biogeography of *Phlebarachnium*. inferred from the EukBank dataset (Berney et al. 2023) on samples with a marine identifier. **(A)** World map showing the different sampling stations (black dots) and maximum contribution of *Phlebarachnium*. to the total eukaryotic community (blue dots) per locality. **(B)** Relative abundance of *Phlebarachnium*. across the latitudinal gradient. **(C)** Depth profile of *Phlebarachnium*. across the longitudinal gradient. **(D)** Graphical representation of the similarity identity

(computed with vsearch: 'allpairs_global'; and represented by the grey gradient lines, or edges) between all *Phlebarachnium* sequences (coloured squares, or nodes) used in this study. Blue nodes represent the D1+D2 regions of the 28S rDNA sequenced in this study, green nodes represent the near full-length rDNA from [35], and orange represent the V4 hypervariable region of the 18S rDNA from eukBank [28]. Note the light orange node representing the third closest hit to our reference sequences, and confidentially showing the taxonomic assignment of *Phlebarachnium* used in this study.

Discussion

Here, we identified the genus *Phlebarachnium*, a distinct Nassellaria clade showing a characteristic gelatinous matrix surrounding the cells and mostly abundant in oligotrophic waters. *Phlebarachnium* is to our knowledge the only solitary lineage of Radiolaria with a gelatinous matrix that diversified independently of other matrix forming Radiolaria (i.e. Orodaria and Collodaria). Despite their distant relationship within the Nassellaria, *Phlebarachnium*, Orodaria and Collodaria share the adaptation of producing a gelatinous matrix and affinity towards oligotrophic zones. Orodaria, is restricted to oligotrophic deep waters, predominantly found in the Pacific Ocean, and lacks symbiotic algae within its gelatinous matrix [22]. Collodaria exhibits high abundance and diversity in shallow, oligotrophic waters [53], a trait attributed to the presence of numerous symbionts scattered in the gelatinous matrix of the colonies [30]. Other Radiolaria groups, such as Acantharia, do not possess a gelatinous matrix but still host numerous photosymbionts [26]. Since Acantharia are rarely found in oligotrophic waters, here we argue that the gelatinous matrix could be a specific innovation to cope with nutrient-poor systems. The gelatinous matrix would increase the volume-to-body weight ratio, facilitating the hosting of a larger number of symbionts and establishing a particular microenvironment that favours the viability of these organisms under conditions of nutrient depletion. Additionally, the increased volume-to-body weight ratio would improve the chances of prey encountering and/or scavenging nutrients for mineralization of the skeleton and/or symbiont nourishment. In addition, the gelatinous matrix may play an important role for buoyancy, especially in Orodaria specimens, which are mostly found in the mesopelagic. Altogether, the gelatinous matrix seems to be a convergent adaptation to oligotrophic waters, where other Radiolaria relatives are rare.

Other protists have also developed sophisticated behaviors to enhance encounter rates. Some dinoflagellates can build a mucosphere with the capacity to attract and immobilize diverse microbes, facilitating subsequent prey selection [54]. In other Radiolaria groups, comparable independent innovations in life mode and morphology have already been hypothesized and

343 documented. Nassellaria's closest relative, Spumellaria, experienced a substantial increase in
344 planar forms during the second half of the Mesozoic, (ca. 145 Mya), which is thought to have
345 resulted from low nutrient availability favoring an increase in the surface/volume ratio [8]. During
346 the same geological epoch, Acantharia, established a photosymbiotic relationship with the
347 Haptophyte *Phaeocystis* [5]. In such a relationship, photosymbionts of Acantharia exhibit plastidal
348 volumes 38-fold larger than those of free-living *Phaeocystis* [26].

349 In the case of Acantharia, their photosymbionts are located inside the cytoplasm [26], whereas
350 Collodaria harbors their photosymbionts scattered in the gelatinous matrix. To our knowledge,
351 Collodaria has not been documented without symbionts [53]. Moreover, some Collodaria have
352 been shown to control the physiology and perhaps the life cycle of their photosymbionts to an
353 extent [27]. In the yellow population of *Phlebarachnium* studied here, the symbionts were
354 strategically arranged, forming discrete clusters within the host's gelatinous matrix, suggesting an
355 active host-mediated placement. In contrast, in the orange population, the symbionts were evenly
356 distributed throughout the matrix. Despite morphological variations among *Phlebarachnium*
357 specimens, DNA barcoding and environmental molecular diversity showed identical sequences
358 in all specimens studied here. Regardless of differences in symbiont distribution within their hosts,
359 all specimens of *Phlebarachnium* hosted round, golden-yellow bodies scattered in the gelatinous
360 matrix. Molecular analyses identified such bodies as *Scrippsiella* (Peridiniales, Dinophycea), a
361 common planktonic symbiont of the jellyfish *Velella velella* [48] and also seen in symbiosis with
362 Acantharia [5], but never before reported in Polcystines Radiolaria [23, 24]. However, given the
363 broad symbiotic interactions among the Dinophycea group and the long divergence time of
364 *Phlebarachnium* (>100 Mya to the last common ancestor of the closest relative), it is plausible
365 that they developed a symbiotic relationship with a different group.

366 In addition to playing a central role in resource acquisition and harbouring symbionts, the matrix
367 also could be important in prey capture. Nassellaria has cytoplasmic extensions that emerge from
368 the conical cephalis, forming a web of cytoplasmic filaments where prey are captured [55]. In the
369 collected specimens, we observed a multitude of enclosed prey within the gelatinous matrix,
370 predominantly copepods of the order Harpacticoida and nauplius larvae. Pelagic harpacticoids,
371 such as *Microsetella* sp., are often associated with marine snow and aggregates in offshore areas
372 where suspended food is scarce , similar to the waters where the *Phlebarachnium* specimens of
373 this study were collected. The consistent occurrence of prey in the gelatinous matrix beneath the
374 cephalis suggests that *Phlebarachnium* may play a relevant role in pelagic food webs by preying

375 on larger metazoan taxa. This is particularly notable in oligotrophic waters, where *Phlebarachnium*
376 seems to be endemic and prey are scarce.

377 In our study we found *Phlebarachnium* in high relative abundances in oligotrophic waters, even
378 in specimens collected at deeper depths (0-300 m). Metabarcoding analyses show that
379 *Phlebarachnium* reaches high relative abundances in the mesopelagic zone (200-1000m), where
380 light penetration is limited and possibly insufficient for the functionality of the symbionts'
381 photosynthesis. Taking into account the significant high relative abundance below 500 m around
382 -160° longitude, this implies that these organisms may be versatile, thriving solely through
383 heterotrophy without relying on photosynthesis. However, oligotrophic clear waters display
384 relatively deep chlorophyll maximas (Fig. 1B) and thus photosynthesis is found at deeper
385 environments regarding nutrient enriched waters. Collodaria has already been shown to inhabit
386 ocean areas where other Radiolaria relatives are rare [30, 43]. In tropical and subtropical nutrient-
387 depleted surface waters, Collodaria can reach up to 1.6×10^4 - 2.0×10^4 colonies per m^3 [59, 60].
388 In our study, *Phlebarachnium* sequences reached maximum abundances of 13.4% relative to the
389 total eukaryotic community reads, especially towards the upper mesopelagic. In this context,
390 *Phlebarachnium* likely thrives in deeper water layers than Collodaria, establishing a distinct
391 ecological niche. The access to this environment allowed them to become important contributors
392 to the planktonic food web of an ecosystem with potentially low predators. However, caution is
393 required when interpreting metabarcoding data [61, 62]. Life cycle of Radiolaria remains poorly
394 understood, with the belief that the release of small bi-flagellated cells (referred to as swarmers)
395 by mature cells plays a role in their reproductive cycle [63, 64]. These swarmers, which could sink
396 to the deep ocean, might contribute to the elevated metabarcoding reads observed in the deep
397 ocean. Additionally, there is a possibility that they become incorporated into sinking particles upon
398 their death.

399 The high abundance and local endemism of *Phlebarachnium* to oligotrophic waters makes them
400 useful candidates for paleoenvironmental reconstruction studies. Their bloom-like presence might
401 reflect an important role in biogeochemical cycles. Considering climate change and expansion of
402 oligotrophic waters in certain oceanic regions [65], the gelatinous matrix could be an enormous
403 advantage for these organisms. Specializing in resource-poor waters could allow *Phlebarachnium*
404 to expand into novel ecological niches, such as different habitats or trophic modes and adapt to
405 novel environmental conditions. It has already been observed that ocean warming can trigger
406 major shifts in the geographic distribution due to the combined effects of warming, stratification,
407 light, nutrients and predation, in a wide range of organisms, from phytoplankton to mammals [66,

67]. In fact, the extensive fossil record of Radiolaria has already shown that rapid climate changes can lead to extinction of specific groups [68]. It is therefore critical to understand whether adaptations, such as the development of a gelatinous matrix, can help certain organisms cope with the rapid changes in ocean chemistry and temperature expected due to anthropogenic activity.

Our study highlights that the presence of a gelatinous matrix was an original convergent evolution of Nassellaria to cope with oligotrophy in the oceans. Studying the exact role of the matrix in these organisms is of particular importance to better understand biodiversity and adaptation of Radiolaria. In particular, investigating the genes responsible for its formation and its chemical composition (i.e., the amount of lipids and carbohydrates) may help to further understand its relationship with symbionts, prey and the host cell. Here we postulate that the gelatinous matrix might be an advantageous trait to adapt to oligotrophic conditions by increasing the effective body size and creating an advantageous microenvironment for symbionts. Such increase in size might thus allow them to host more photo-symbionts than their relatives without a gelatinous matrix and similar body weight and further digest prey. This study not only advances our understanding in the ecological strategies of Radiolaria but also offers insights into the broader dynamics of organisms flourishing in nutrient-limited ecosystems.

Author contributions

NLM and ML collected the samples. NLM and MMS conceived the presented idea, participated in the conceptualization, planned and performed the analyses, prepared the figures and wrote the manuscript. SR carried out the DNA extraction, amplification and purification. NLL, ML, SR, YN, TB and MMS commented and revised the manuscript.

Acknowledgments

The authors would like to thank the captain and crew of the R/V *Roger Revelle* of the Scripps Institution of Oceanography for their expertise and support. We also thank colleagues within the CCE-LTER program (National Science Foundation grants OCE-1637632 and OCE-1614359) who contributed to sample collection and its lead PIs Katherine Barbeau and Mark Ohman. This work was supported by the “Agence Nationale de la Recherche” project RhiCycle (ANR-19-CE01-0006) granted to TB and the ISblue project RHICE (ANR-17-EURE-0015) . NLL received funding from the European Union’s Horizon Europe research and innovation programme under grant agreement No 101064167 (MSCA postdoctoral fellowship Si-ORHIGENS). MMS was supported by a postdoctoral fellowship from the Beatriu de Pinós programme of the Government of Catalonia's Secretariat for Universities and Research of the Generalitat de Catalunya Economy and Knowledge (grant number: 2021BP00068). We would like to express our gratitude to Aude Leynaert for support, Fabrice Not for providing lab space and resources, ABiMs for computational resources, Johan Renaudie for the taxonomic contribution, Nicolas Henry for advising us on biogeographic analyses, Ian Probert for discussions on the nature of the symbionts and Steve Cunningham for SEM support. We are also very grateful to Colleen Durkin and Daniel Richter for their valuable input and advice on earlier versions of this manuscript.

Supplementary Material

Supplementary tables headers

Table S1. Morphological measurements, major and minor axes of individual cells, and their skeleton and gelatinous matrix areas.

Table S2. List of specimens used for phylogenetic analysis.

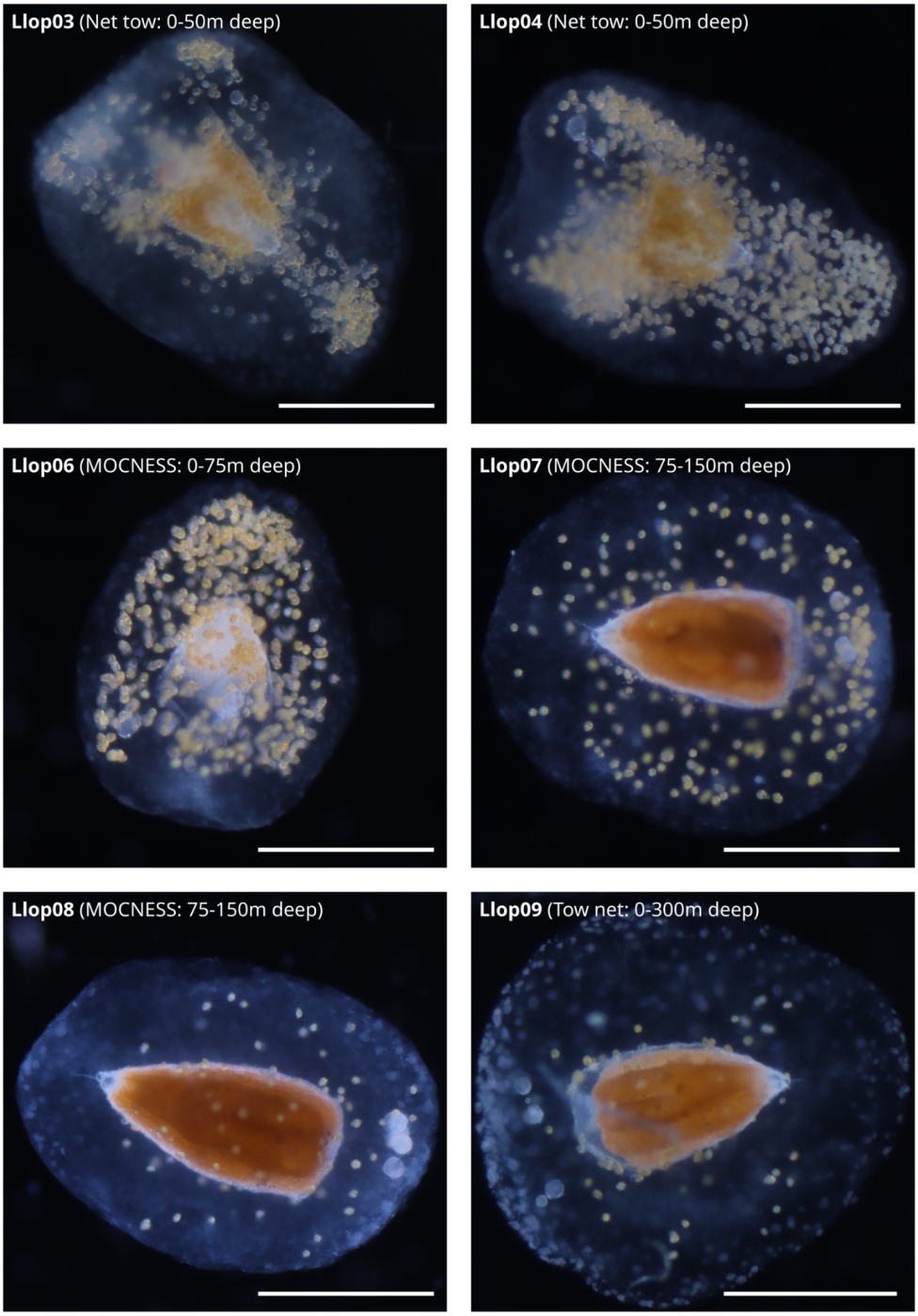

Fig. S1 Light microscope images of live *Phlebarachnium* specimens used in this study for phylogenetic analysis in Fig. 3. Scale bar represents 500 μm.

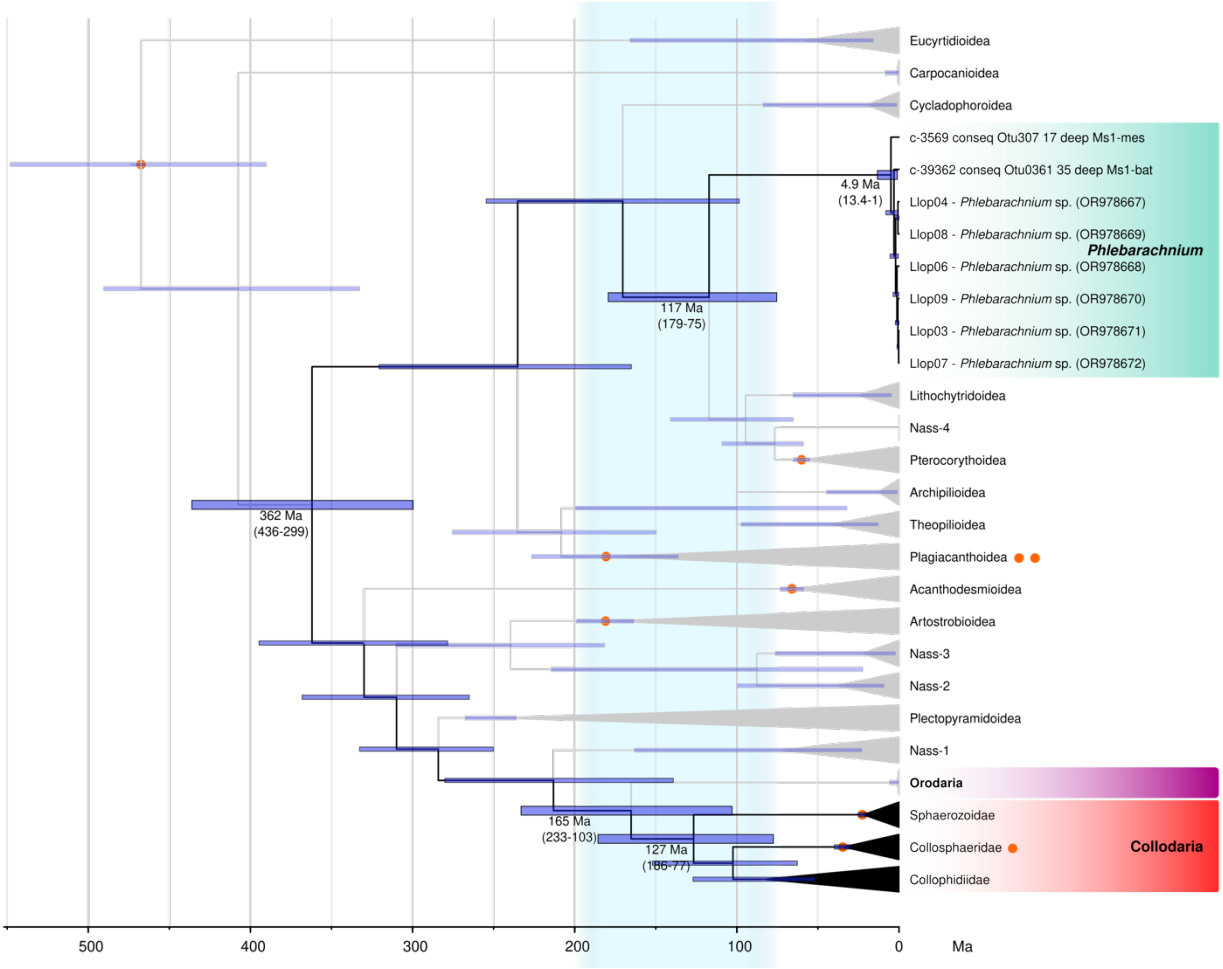

Fig. S2 Time-calibrated tree (Molecular clock) of Nassellaria highlighting the divergence time between the two groups producing a gelatinous matrix, based on the alignment matrix used for phylogenetic analyses (Fig. 3). Divergence times were inferred under an optimized relaxed clock model and GTR+G for 3 independent chains of 100M cycles sampled every 1000 steps and a 25% burnin, implemented in the software package BEAST2. Twelve different nodes were selected for the calibration (orange dots, including the outgroup, Spumellaria), based on [43], with the exception of the root in which a uniform distribution (with minimum of 500 and maximum of 1200 Ma) was used. Blue bars indicate the 95% highest posterior density (HPD) intervals of the posterior probability distribution of node ages.

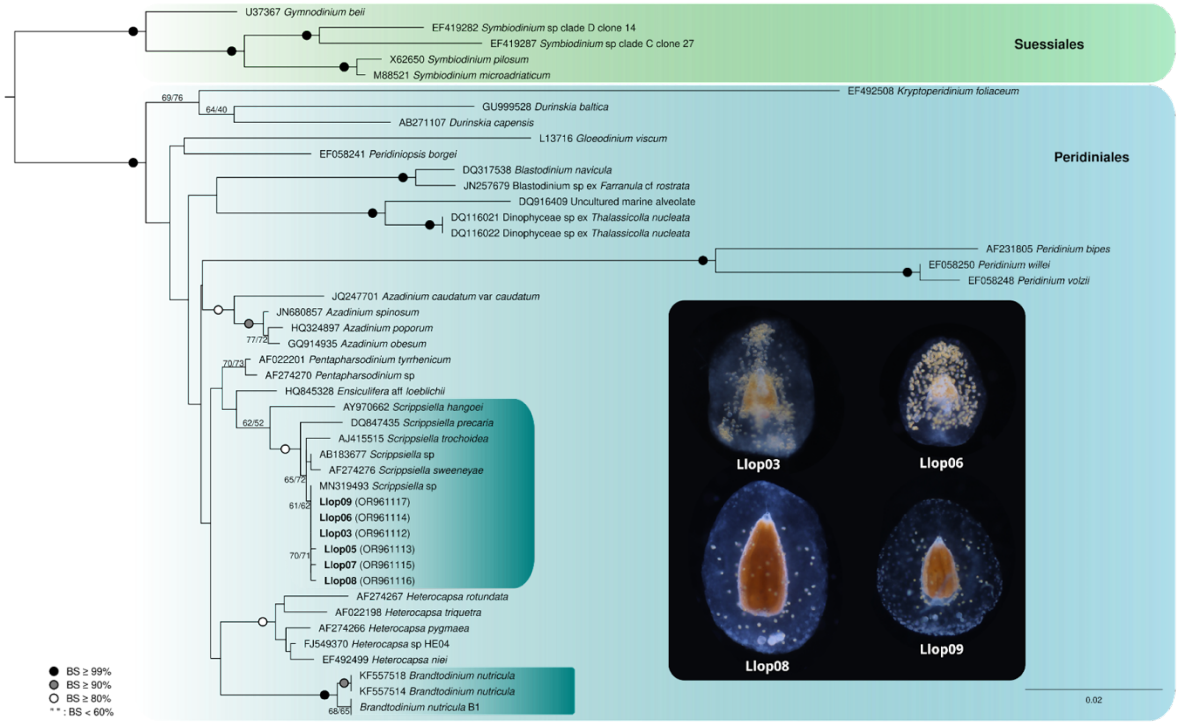

Fig. S3 Molecular phylogeny of Peridiniales, with special focus on symbiotic dinoflagellates inferred from the 18S rDNA (71 taxa and 1803 aligned positions) using the sequences published in Probert et al., (2014) as reference. Values at nodes represent RAxML-ng (GTR+Gamma; tree shown in figure) and IQ-Tree (GTR+F+F4) bootstrap values (BS; 1000 bootstrap each). Only values above 60 BS are shown. Hollow circles at nodes indicate BS ≥ 80, filled grey circles BS ≥ 90 and filled black circles BS ≥ 99.

References

1. Biard T, Stemmann L, Picheral M, Mayot N, Vandromme P, Hauss H, et al. In situ imaging reveals the biomass of giant protists in the global ocean. *Nature* 2016; **532**: 504–507.
2. Pernice MC, Giner CR, Logares R, Perera-Bel J, Acinas SG, Duarte CM, et al. Large variability of bathypelagic microbial eukaryotic communities across the world's oceans. *ISME J* 2015; **10**: 945–958.
3. Suzuki N, Not F. Biology and Ecology of Radiolaria. *Marine protists: diversity and dynamics*. 2015. Springer, Tokyo; New York, pp 179–222.
4. Biard T. Rhizaria. *eLs* 2022.
5. Decelle J, Suzuki N, Mahé F, De Vargas C, Not F. Molecular Phylogeny and Morphological Evolution of the Acantharia (Radiolaria). *Protist* 2012; **163**: 435–450.

6. Takahashi K. Radiolaria: sinking population, standing stock, and production rate. *Marine Micropaleontology* 1983; **8**: 171–181.
7. Sandin MM, Biard T, Romac S, O'Dogherty L, Suzuki N, Not F. A Morpho-molecular Perspective on the Diversity and Evolution of Spumellaria (Radiolaria). *Protist* 2021; **172**: 125806.
8. Sandin MM, Pillet L, Biard T, Poirier C, Bigeard E, Romac S, et al. Time Calibrated Morpho-molecular Classification of Nassellaria (Radiolaria). *Protist* 2019; **170**: 187–208.
9. Biard T, Pillet L, Decelle J, Poirier C, Suzuki N, Not F. Towards an Integrative Morpho-molecular Classification of the Collodaria (Polycystinea, Radiolaria). *Protist* 2015; **166**: 374–388.
10. Nakamura Y, Tuji A, Kimoto K, Yamaguchi A, Hori RS, Suzuki N. Ecology, Morphology, Phylogeny and Taxonomic Revision of Giant Radiolarians, Orodaria ord. nov. (Radiolaria; Rhizaria; SAR). *Protist* 2021.
11. Lampitt RS, Briggs N, Cael BB, Espinola B, Hélaouët P, Henson SA, et al. Deep ocean particle flux in the Northeast Atlantic over the past 30 years: carbon sequestration is controlled by ecosystem structure in the upper ocean. *Front Earth Sci* 2023; **11**: 1176196.
12. Laget M, Llopis Monferrer N, Maguer J, Leynaert A, Biard T. Elemental content allometries and silicon uptake rates of planktonic Rhizaria: Insights into their ecology and role in biogeochemical cycles. *Limnology & Oceanography* 2023; **68**: 439–454.
13. Drago L, Panaïotis T, Irisson J-O, Babin M, Biard T, Carlotti F, et al. Global Distribution of Zooplankton Biomass Estimated by In Situ Imaging and Machine Learning. *Front Mar Sci* 2022; **9**: 894372.
14. Laget M, Drago L, Panaïotis T, Kiko R, Stemmann L, Rogge A, et al. Global census of the significance of giant mesopelagic protists to the marine carbon and silicon cycles. *Under review* .
15. Gutierrez-Rodriguez A, Stukel MR, Lopes dos Santos A, Biard T, Scharek R, Vaulot D, et al. High contribution of Rhizaria (Radiolaria) to vertical export in the California Current Ecosystem revealed by DNA metabarcoding. *ISME J* 2018; **13**: 964–976.
16. Preston CM, Durkin CA, Yamahara KM. DNA metabarcoding reveals organisms contributing to particulate matter flux to abyssal depths in the North East Pacific ocean. *Deep Sea Research Part II: Topical Studies in Oceanography* 2020; **173**: 104708.
17. Llopis Monferrer N, Boltovskoy D, Tréguer P, Sandin MM, Not F, Leynaert A. Estimating Biogenic Silica Production of Rhizaria in the Global Ocean. *Global Biogeochem Cycles* 2020; **34**.
18. Tréguer PJ, Sutton JN, Brzezinski MA, Charette MA, Devries T, Dutkiewicz S, et al. Reviews and syntheses: The biogeochemical cycle of silicon in the modern ocean. *Biogeosciences* 2021.
19. De Wever P, Dumitrica P, Caulet JP, Nigrini C, Caridroit M. Radiolarians in the Sedimentary Record. 2001. CRC Press, London.
20. Lazarus D, Suzuki N, Ishitani Y, Takahashi K. Paleobiology of the Polycystine Radiolaria, 1st ed: Hoboken. 2021. NJ: Wiley-Blackwell.
21. Civel-Mazens M, Crosta X, Cortese G, Michel E, Mazaud A, Ther O, et al. Antarctic Polar Front migrations in the Kerguelen Plateau region, Southern Ocean, over the past 360 kyrs. *Global and Planetary Change* 2021; **202**: 103526.
22. Nakamura Y, Itagaki H, Tuji A, Shimode S, Yamaguchi A, Hidaka K, et al. DNA metabarcoding focused on difficult-to-culture protists: An effective approach to clarify biological interactions. *Environmental Microbiology* 2023; 1462-2920.16524.
23. Probert I, Siano R, Poirier C, Decelle J, Biard T, Tuji A, et al. *B randtodinium* gen. nov. and *B . nutricula* comb. Nov. (Dinophyceae), a dinoflagellate commonly found in symbiosis with polycystine radiolarians. *J Phycol* 2014; **50**: 388–399.

24. Yuasa T, Horiguchi T, Mayama S, Takahashi O. *Gymnoxanthella radiolariae* gen. et sp. nov. (Dinophyceae), a dinoflagellate symbiont from solitary polycystine radiolarians. *Journal of Phycology* 2016; **52**: 89–104.
25. Mitra A, Caron DA, Faure E, Flynn KJ, Leles SG, Hansen PJ, et al. The Mixoplankton Database (MDB): Diversity of photo-phago-trophic plankton in form, function, and distribution across the global ocean. *J Eukaryotic Microbiology* 2023; **70**: e12972.
26. Decelle J, Stryhanyuk H, Gallet B, Veronesi G, Schmidt M, Balzano S, et al. Algal Remodeling in a Ubiquitous Planktonic Photosymbiosis. *Current Biology* 2019; **29**: 968-978.e4.
27. Decelle J, Veronesi G, LeKieffre C, Gallet B, Chevalier F, Stryhanyuk H, et al. Subcellular architecture and metabolic connection in the planktonic photosymbiosis between Collodaria (radiolarians) and their microalgae. *Environmental Microbiology* 2021; **23**: 6569–6586.
28. Michaels AF. Acantharian abundance and symbiont productivity at the VERTEX seasonal station. *J Plankton Res* 1991; **13**: 399–418.
29. Michaels AF. Vertical distribution and abundance of Acantharia and their symbionts. *Marine Biology* 1988; **97**: 559–569.
30. Faure E, Not F, Benoiston A-S, Labadie K, Bittner L, Ayata S-D. Mixotrophic protists display contrasted biogeographies in the global ocean. *ISME J* 2019; **13**: 1072–1083.
31. Lipsman V, Shlakhter O, Rocha J, Segev E. Bacteria Contribute Exopolysaccharides to an Algal-Bacterial Joint Extracellular Matrix. *bioRxiv* 2023.
32. Brisbin MM, Mitarai S, Saito MA, Alexander H. Microbiomes of bloom-forming *Phaeocystis* algae are stable and consistently recruited, with both symbiotic and opportunistic modes. *The ISME Journal* 2022; **16**: 2255–2264.
33. Strelkov AA, Reshetnyak VV. A New Life Form in Radiolarians. *Zoological Journal* 1959; **38**.
34. Suzuki N, O'Dogherty L, Caulet JP, Dumitrica P. New integrated morpho- and molecular systematic classification of Cenozoic radiolarians (Class Polycystinea) – suprageneric taxonomy and logical nomenclatorial acts, in O'dogherty L. (ed.), Catalog of Cenozoic radiolarians. *Geodiversitas* 2021; **43**: 405–573.
35. Berney C, Fréderic M, Henry N, Enrique L, De Vargas C, Eubank consortium. EukBank 18S V4 dataset. 2023. Zenodo.
36. Schneider CA, Rasband WS, Eliceiri KW. NIH Image to ImageJ: 25 years of image analysis. *Nat Methods* 2012; **9**: 671–675.
37. Abràmoff MD, Magalhães PJ, Sunanda JR. Image Processing with ImageJ. *Biophotonics International* ; **11**: 36–42.
38. Llopis Monferrer N, Foulon V, Elies P. Enhanced scanning electron microscopy images using muscovite mica, an example with Rhizaria. *Microscopy Res & Technique* 2022; **85**: 2748–2751.
39. Schloss PD, Westcott SL, Ryabin T, Hall JR, Hartmann M, Hollister EB, et al. Introducing mothur: Open-Source, Platform-Independent, Community-Supported Software for Describing and Comparing Microbial Communities. *Appl Environ Microbiol* 2009; **75**: 7537–7541.
40. Guillou L, Bachar D, Audic S, Bass D, Berney C, Bittner L, et al. The Protist Ribosomal Reference database (PR2): a catalog of unicellular eukaryote Small Sub-Unit rRNA sequences with curated taxonomy. *Nucleic Acids Research* 2013; **41**: D597–D604.
41. Jamy M, Biwer C, Vaulot D, Obiol A, Jing H, Peura S, et al. Global patterns and rates of habitat transitions across the eukaryotic tree of life. *Nat Ecol Evol* 2022; **6**: 1458–1470.

42. Rognes T, Flouri T, Nichols B, Quince C, Mahé F. VSEARCH: a versatile open source tool for metagenomics. *PeerJ* 2016; **4**: e2584.
43. Sandin MM, Renaudie J, Suzuki N, Not F. Beyond the stars of the ocean: Diversity and evolution of Radiolaria. *In prep* .
44. Katoh K, Standley DM. MAFFT Multiple Sequence Alignment Software Version 7: Improvements in Performance and Usability. *Molecular Biology and Evolution* 2013; **30**: 772–780.
45. Larsson A. AliView: a fast and lightweight alignment viewer and editor for large datasets. *Bioinformatics* 2014; **30**: 3276–3278.
46. Capella-Gutiérrez S, Silla-Martínez JM, Gabaldón T. trimAl: a tool for automated alignment trimming in large-scale phylogenetic analyses. *Bioinformatics* 2009; **25**: 1972–1973.
47. Kozlov AM, Darriba D, Flouri T, Morel B, Stamatakis A. RAxML-NG: a fast, scalable and user-friendly tool for maximum likelihood phylogenetic inference. *Bioinformatics* 2019; **35**: 4453–4455.
48. Minh BQ, Schmidt HA, Chernomor O, Schrempf D, Woodhams MD, Von Haeseler A, et al. IQ-TREE 2: New Models and Efficient Methods for Phylogenetic Inference in the Genomic Era. *Molecular Biology and Evolution* 2020; **37**: 1530–1534.
49. Ronquist F, Teslenko M, Van Der Mark P, Ayres DL, Darling A, Höhna S, et al. MrBayes 3.2: Efficient Bayesian Phylogenetic Inference and Model Choice Across a Large Model Space. *Systematic Biology* 2012; **61**: 539–542.
50. Bouckaert R, Vaughan TG, Barido-Sottani J, Duchêne S, Fourment M, Gavryushkina A, et al. BEAST 2.5: An advanced software platform for Bayesian evolutionary analysis. *PLoS Comput Biol* 2019; **15**: e1006650.
51. Douglas J, Zhang R, Bouckaert R. Adaptive dating and fast proposals: Revisiting the phylogenetic relaxed clock model. *PLoS Comput Biol* 2021; **17**: e1008322.
52. Gernhard T. The conditioned reconstructed process. *Journal of Theoretical Biology* 2008; **253**: 769–778.
53. Biard T, Bigeard E, Audic S, Poulain J, Gutierrez-Rodriguez A, Pesant S, et al. Biogeography and diversity of Collodaria (Radiolaria) in the global ocean. *ISME J* 2017; **11**: 1331–1344.
54. Larsson ME, Bramucci AR, Collins S, Hallegraeff G, Kahlke T, Raina J-B, et al. Mucospheres produced by a mixotrophic protist impact ocean carbon cycling. *Nat Commun* 2022; **13**: 1301.
55. Anderson OR, Swanberg NR, Bennett P. An estimate of predation rate and relative preference for algal versus crustacean prey by a spongiose skeletal radiolarian. *Mar Biol* 1984; **78**: 205–207.
56. Ohtsuka S, Kubo N, Okada M, Gushima K. Attachment and feeding of pelagic copepods on larvacean houses. *J Oceanogr* 1993; **49**: 115–120.
57. Uye S. Seasonal population dynamics and production of Microsetella norvegica, a widely distributed but little-studied marine planktonic harpacticoid copepod. *Journal of Plankton Research* 2002; **24**: 143–153.
58. Koski M, Kiørboe T, Takahashi K. Benthic life in the pelagic: Aggregate encounter and degradation rates by pelagic harpacticoid copepods. *Limnol Oceanogr* 2005; **50**: 1254–1263.
59. Swanberg NR, Caron DA. Patterns of sarcodine feeding in epipelagic oceanic plankton. *J Plankton Res* 1991; **13**: 287–312.

60. Dennett MR. Video plankton recorder reveals high abundances of colonial Radiolaria in surface waters of the central North Pacific. *Journal of Plankton Research* 2002; **24**: 797–805.
61. Llopis Monferrer N, Biard T, Sandin MM, Lombard F, Picheral M, Elineau A, et al. Siliceous Rhizaria abundances and diversity in the Mediterranean Sea assessed by combined imaging and metabarcoding approaches. *Front Mar Sci* 2022; **9**: 895995.
62. Sandin MM, Romac S, Not F. Intra-genomic RRNA gene variability of Nassellaria and Spumellaria (Rhizaria, Radiolaria) assessed by Sanger, MINION and Illumina sequencing. *Environmental Microbiology* 2022; **24**: 2979–2993.
63. Anderson OR, Swanberg NR, Bennett P. Assimilation of symbiont-derived photosynthates in some solitary and colonial radiolaria. *Mar Biol* 1983; **77**: 265–269.
64. Yuasa T, Takahashi O. Ultrastructural morphology of the reproductive swarmers of Sphaerozoum punctatum (Huxley) from the East China Sea. *European Journal of Protistology* 2014; **50**: 194–204.
65. Leonelli FE, Bellacicco M, Pitarch J, Organelli E, Buongiorno Nardelli B, De Toma V, et al. Ultra-Oligotrophic Waters Expansion in the North Atlantic Subtropical Gyre Revealed by 21 Years of Satellite Observations. *Geophysical Research Letters* 2022; **49**: e2021GL096965.
66. Albouy C, Delattre V, Donati G, Frölicher TL, Albouy-Boyer S, Leprieur F. Global vulnerability of marine mammals to global warming. *Scientific Reports* 2020.
67. Benedetti F, Vogt M, Hofmann Elizondo U, Righetti D, Zimmermann NE, Gruber N. Major restructuring of marine plankton assemblages under global warming. *Nature Communications* 2021.
68. Trubovitz S, Lazarus D, Renaudie J, Noble PJ. Marine plankton show threshold extinction response to Neogene climate change. *Nat Commun* 2020; **11**: 5069.